Available online at www.sciencedirect.com
ScienceDirect
Geomorphology 95 (2008) 412–428
GEOMORPHOLOGY
www.elsevier.com/locate/geomorph

Meteorological causes of Harmattan dust in West Africa

Wolfgang Schwanghart *, Brigitta Schütt

Institute of Geographic Sciences, Freie Universität Berlin, Malteserstr. 74-100, D-12249 Berlin, Germany

Received 11 October 2006; received in revised form 24 April 2007; accepted 15 July 2007
Available online 20 July 2007

Abstract

We investigated the temporal dynamics of dust entrainment in the Bodélé Depression, Central Sahara, to better understand the intra-annual variability of aerosol emission in the world's largest dust source. The linkages between dust entrainment and large-scale meteorological factors were examined by correlating several meteorological variables in the Mediterranean and Africa north of the equator with the aerosol concentrations in the Bodélé Depression separately for winter and summer. The methodological tools applied are NCEP/NCAR reanalysis data and the aerosol index of the Total Ozone Mapping Spectrometer (TOMS-AI), available for 15 years from 1978 to 1993. We found that dust mobilisation during the Harmattan season is highly dependent on air pressure variability in the Mediterranean area. High pressure to the north of the Bodélé intensifies the NE trade winds, leading to an increased entrainment of dust in the Bodélé Depression. In summer, dust mobilization cannot be explained by the large scale meteorological conditions. This highlights the importance of local to regional wind systems linked to the northernmost position of the intertropical convection zone (ITCZ) during this time.
© 2007 Elsevier B.V. All rights reserved.

Keywords: NCEP/NCAR reanalysis; TOMS-AI; Synoptic climatology; Bodélé; Aerosol; Dust; West Africa; Aeolian dynamics

1. Introduction

Mineral dust is a crucial factor in the Earth's climate system and impacts on nutrient dynamics and biogeochemical cycling of oceanic and terrestrial ecosystems (Péwé, 1981; Arimoto, 2001; Middleton and Goudie, 2001; Griffin et al., 2004; Engelstaedter et al., 2006). Entrained from sediments or soils, it can be transported by the wind for several thousands of kilometres. The Bodélé Depression in the Republic of Chad has been found to be the world's largest source of mineral dust (Herrmann et al., 1999; Brooks and Legrand, 2000; Goudie and Middleton, 2001; Prospero et al., 2002; Giles, 2005; Washington et al., 2003). Dust entrained in this basin is transported over great distances as far as the Caribbean Sea, the Amazon Basin, the United States and Europe (Schütz et al., 1981; Prospero, 1999; Dunion and Velden, 2004; Koren et al., 2006).

In Sahelian and Saharan Africa aeolian dust transport is accomplished by several wind systems (Jäkel, 2004; Engelstaedter et al., 2006). One of the most prominent wind systems is the Harmattan (Fig. 1), a ground level stream of dry desert air which is part of the African continental trade wind system that sweeps far southward from a consistent NE direction during the boreal winter (Hastenrath, 1988). During the winter months the seasonally variable Harmattan current transports large

* Corresponding author. Tel.: +49 30 838 70439; fax: +49 30 838 70755.
E-mail address: schwanghart@geog.fu-berlin.de (W. Schwanghart).

0169-555X/$ - see front matter © 2007 Elsevier B.V. All rights reserved.
doi:10.1016/j.geomorph.2007.07.002

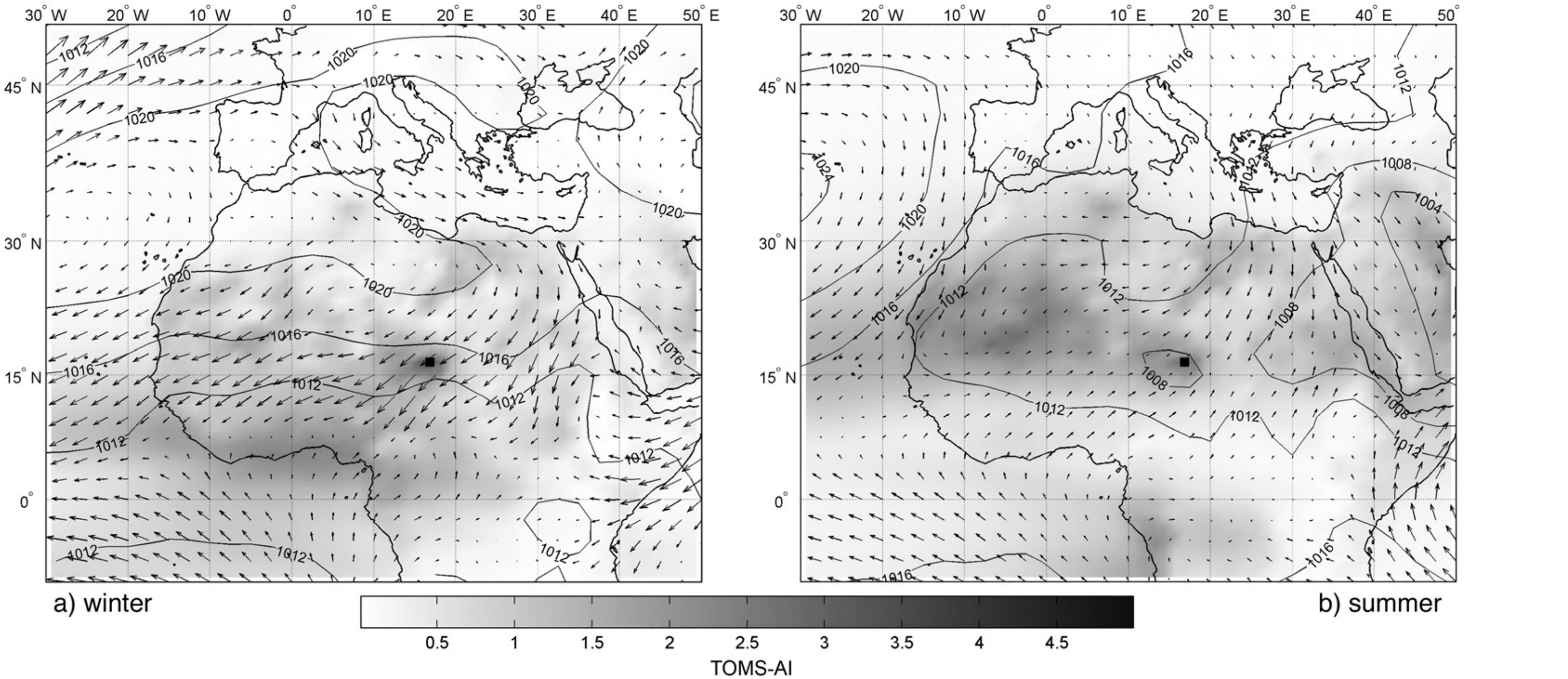

Fig. 1. Mean annual atmospheric mineral dust concentrations quantified by TOMS aerosol index (dimensionless) and NCEP/NCAR horizontal wind vectors at 925 hPa in winter (December to February) and summer (June to August) during the years 1978–1993. The black square indicates the location of the Bodélé Depression.

amounts of mineral dust at irregular intervals from the Chad Basin to the Sahel and Guinean coast where it reduces visibility, relative humidity and temperatures (Kalu, 1979; McTainsh and Walker, 1982; Adedokun et al., 1989; Stahr et al., 1996; Breuning-Madsen and Awadzi, 2005). The increased aerosol concentrations cause irritation of respiratory tracts, and visibility reduction in car and air traffic that represent a serious problem during dust spell events (Middleton, 1997). As a consequence, an airplane crashed in Ivory Coast because the engines were affected by dust in February 2000 (http://www.nrlmry.navy.mil/aerosol/Case_studies/20000130_ivorycoast/, 20.09.2006).

In order to prevent or mitigate the negative ecological and economical effects of mineral aerosols on populations in deserts and desert-fringe environments, the understanding of the geomorphological processes governing atmospheric dust dynamics is of vital interest (Goudie and Middleton, 2001). Geomorphological research of aeolian systems largely focuses on the production of the fine-grained material, the mechanisms of mobilization, transport and deposition, and the effects of wind-blown dust on landform evolution. A better understanding of these processes requires observations, analyses and modelling at different spatial and temporal scales. Since dust entrainment, transport and deposition

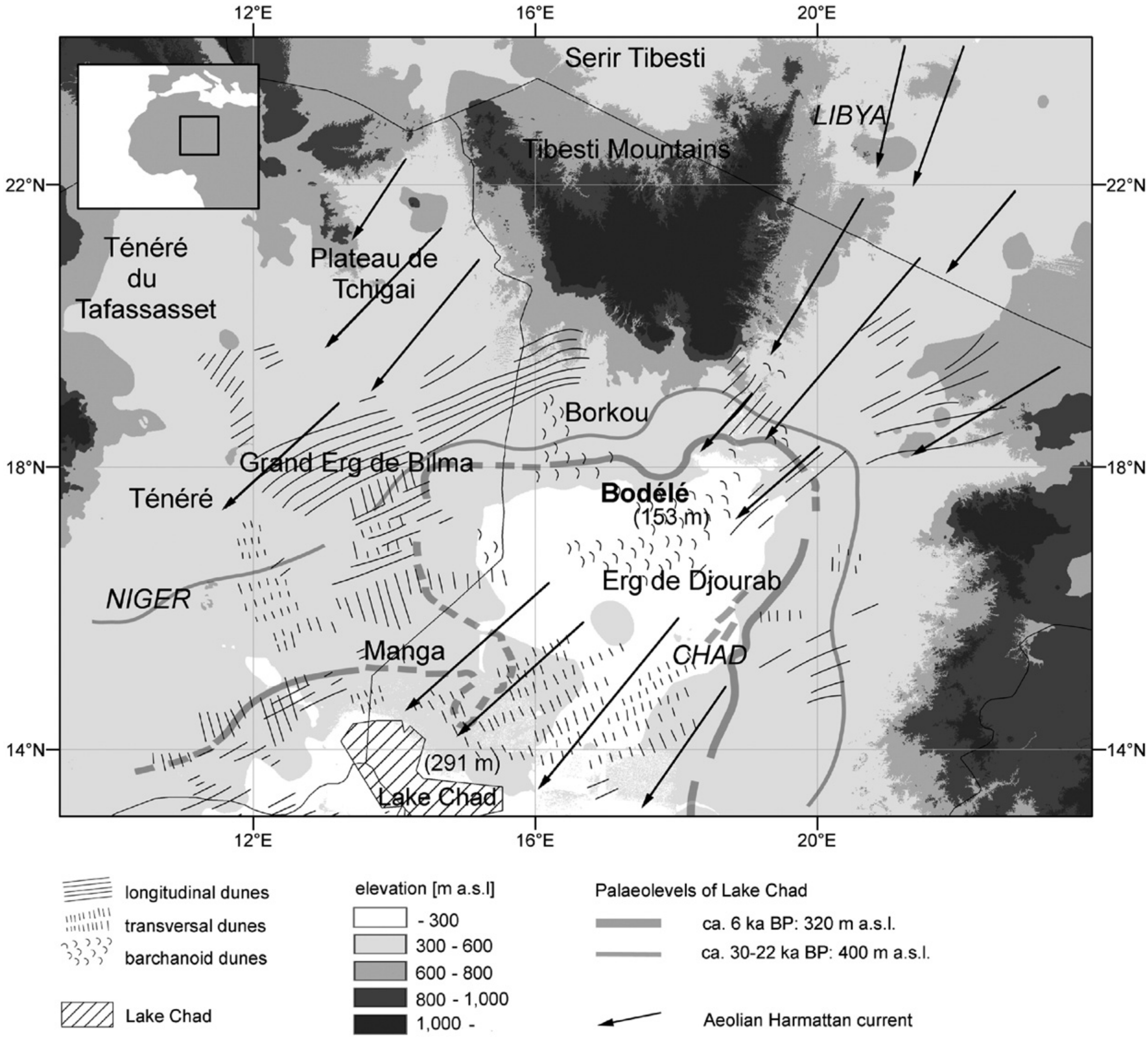

Fig. 2. Regional setting of the Bodélé Depression modified after Grove and Warren (1968), Mainguet (1996) and Pachur and Altmann (2006). Elevation data are based on GTOPO30.

are closely connected to meteorological processes, the investigation of these processes necessitates a multidisciplinary approach.

The study presented in this paper is to be placed at the interface of geomorphology and meteorology. We concentrated on the short-term variability of dust emissions of the Bodélé Depression and tried to explain it with existing large-scale meteorological datasets. The underlying idea is that geomorphological processes of short-term and small-scale fluctuations in dust mobilisation mainly depend on wind speed and surface roughness (Gillette and Chen, 1999). The small-scale meteorological processes, however, are related to the regional and large-scale meteorological conditions, which can be characterised by existing datasets and can be forecasted. Due to the seasonality in the pressure and wind systems, the influences should differ during the most diverse seasons: summer and winter. Hence, we investigated the seasonality in the meteorological impact on dust emission in the Bodélé Depression. The derived information on the relation between the large-scale meteorological conditions and dust entrainment in a local area can contribute to predicting the hazardous weather events caused by atmospheric dust.

Most recently, Washington and Todd (2005) and Washington et al. (2006) showed that the low level jet (LLJ) is an important control on dust emission in the Bodélé Depression. In this paper we provide evidence that day-to-day variability of dust emission in the Bodélé Depression can be explained by the LLJ using an extensive dataset characterising large-scale meteorological factors, defined as the state of the atmospheric conditions with a duration of one to several days.

2. Regional setting

The Bodélé Depression is located in the Central Sahara around 17°N and 18°E northeast of Lake Chad. With its lowest elevation at 153 m a.s.l., the Bodélé Depression represents the lowest part of the Chad Basin (Fig. 2) and adjoins the Tibesti Mountains in the north, the Erg de Bilma in the west and the Erg du Djourab in the south. With an estimated annual precipitation of less than 10 mm, the climate in the Bodélé Depression can be characterized as hyper arid (Washington and Todd, 2005).

The reason for today's significance of the Bodélé Depression as a dust source can be found in its history. Its development is highly connected to the evolution of Lake Chad showing enormous lake level fluctuations during the Pleistocene and Holocene, driven by monsoon variability (Fig. 2) (Drake and Bristow, 2006). A well-established chronology of humid and dry phases exists for the last fifty thousand years (Busche, 1998; several authors in Pachur and Altmann, 2006). A domination of freshwater conditions in these lakes caused the sedimentation of diatomite, which today is either near the surface or partly covered by sands of the latest aeolian accumulation phase. According to the Saharo-Sahelian Global Wind Action System of Mainguet (1996) these sands are part of an aeolian sand stream following the predominant NE-SW direction of the near-surface trade winds connecting deflation and accumulation areas in the Sahara.

3. Methods

In order to understand the influence of large-scale meteorological factors on dust mobilisation we analysed the correlation of two data sets covering the period from 1978 to 1993.

Aerosol in the atmosphere was quantified using the level-3 aerosol index (version 8) of the Total Ozone Mapping Spectrometer (TOMS-AI) on the Nimbus satellite. TOMS-AI is a measure of how much the wavelength dependence of back-scattered UV radiation from an atmosphere containing aerosols differs from that of a pure Rayleigh atmosphere (Herman et al., 1997; McPeters et al., 1998; Chiapello et al., 1999). Because of different absorptivity at UV wavelengths due to particle size and form TOMS-AI allows us to distinguish between mineral dust and smoke, both over land and sea. Negative index values indicate non-absorbing aerosols such as sulphate aerosols (Chiapello and Moulin, 2002), whereas atmospheric mineral dust concentrations are quantified by positive values. An index value of zero stands for an aerosol free atmosphere. The spectrometer takes measurements almost every single day over most of the Earth's surface with a near-noon equator crossing time. The spatial resolution of the level-3 data is one degree latitude and 1.25 degrees longitude cell size, and the accuracy of the data is set to one decimal place. The data that spans the period November 1978 to May 1993 are archived by NASA and can be downloaded from http://toms.gsfc.nasa.gov. To remove the effect of non-absorbing aerosols on statistics applied in this study, negative TOMS-AI values were set to zero.

To characterise the temporal behaviour of dust emission in the Bodélé Depression, a time series was extracted at 16.5°N, 16.875°E from the daily TOMS-AI grids covering 5301 days including 139 missing values. The location chosen represents the cell centre in the dataset with the maximum mean TOMS-AI value during the period under investigation which underpins the notion of the Bodélé Depression being the largest dust source worldwide. The derived time series was first analyzed in the time domain in order to gain insight into the temporal behaviour and data dependence of the time series. This was achieved using autocorrelation analysis and monthly aggregation of the daily TOMS-AI values. As results from the time domain analysis suggest a rather complex behaviour of the TOMS-AI time series, both in the short- and the long-term (see Results section), the series was further analyzed in the wavelet domain.

Wavelet transform (WT) analysis is a relatively new tool to study multiscale, nonstationary processes occurring over finite temporal domains by decomposing a time series into time-frequency space (Morlet, 1983). Other than Fourier transform that utilizes sine and cosine base functions with infinite span and global uniformity in time, WT uses generalized local base functions, termed wavelets, that can be dilated and translated in both frequency and time (Lau and Weng, 1995; Torrence and Compo, 1997).

Two main categories of wavelet functions can be used in WT: continuous and orthogonal wavelets. Here we applied the continuous Morlet wavelet as “mother wavelet”. This base function has the advantage that its complex nature enables detection of both time-dependent amplitude and phase for different frequencies (Lau and Weng, 1995). WT was applied to the years 1980 to 1992 as the other years of the available data were either incomplete or featured too many missing values (see Fig. 4). Missing values in the remaining series were interpolated linearly prior to WT. The adjustable parameter of the Morlet wavelet was set to eight as this yielded the best resolution level both in time and frequency. The longest time window applied equalled the length of the input time series with 4749 observations. The achieved time frequency spectrum was plotted as magnitude (M) calculated from:

$$M = \sqrt{\mathrm{Re}\{z\}^2 + \mathrm{Im}\{z\}^2}$$

where Re refers to the real component and Im to the imaginary component of the complex Morlet WT z.

The state of the atmosphere was characterised by the intrinsic daily 2.5°×2.5° National Centers for Environmental Prediction/National Center for Atmospheric Research (NCEP/NCAR) Reanalysis Project dataset covering the area between 50°N to 10°S and 30°W to 50°E (IRI/LDEO Climate Data Library, http://iridl.ldeo.columbia.edu). The spatial extent of the data comprises 825 cells and was chosen as it captures the macro-synoptical circulation patterns, including the westerly dynamics in the north and the intertropical convection zone (ITCZ) in the south, and does not overstress computational feasibility. The data are obtained by the reanalysis of the global meteorological network data using a mid-range state-of-the-art weather forecast model (Kalnay et al., 1996). Variables included in the analysis are listed in Table 1.

The relationship between dust mobilisation in the Bodélé Depression and the large-scale meteorological conditions was examined using an extensive correlation analysis with the bivariate Pearson product-moment correlation coefficient r_{xy} as a measure for the strength of the relationship between the time series of TOMS-AI (y) and the time series of each grid cell of NCEP/NCAR variables ($x_{\mathrm{lat,long,var}}$) indexed by its location and meteorological variable.

Applying this basic statistical method to time series becomes challenging, however, due to serial dependence or autocorrelation of the observations in each variable. Serial dependence of successive observations (persistence) is caused by the memorizing ability and inertia of the system under investigation and leads to a biased and thus inaccurate estimation of confidence intervals of statistical parameters such as mean and variance (Mudelsee, 2002, 2003; Politis, 2003). Here, we apply a method proposed by Mudelsee (2003) who employs a stationary non-parametric bootstrap of time series similar to a procedure developed by Politis and Romano (1994) termed block bootstrap. Bootstrapping was developed by Efron (1979) and refers to a method for estimating statistical parameters from a sample by resampling with replacement from the original sample. Bootstrapping does not require any assumptions on the theoretical distribution of the sample and has proven to yield accurate results when working with small samples. However, this method assumes independent and identically distributed (i.i.d.) data (Politis, 2003).

Mudelsee’s (2003) method enhances bootstraping to the non-i.i.d. case by replacing subsampling of single observations by subsampling blocks of subsequent observations in order to estimate the Pearson correlation

Table 1
NCEP/NCAR reanalysis data included in the analysis (Kalnay et al., 1996) and abbreviations used in Figs. 6–9

Variable [unit]	Level [hPa]	Abbreviation
Sea level pressure [hPa]	–	SLP
Zonal & meridional wind component [m/s]	925, 850, 500, 200	WS
Geopotential height [gpm]	850, 500, 200	GPH
Temperature [K]	925, 850, 500, 200	T
Specific humidity [kg/kg]	925, 850, 500	SH

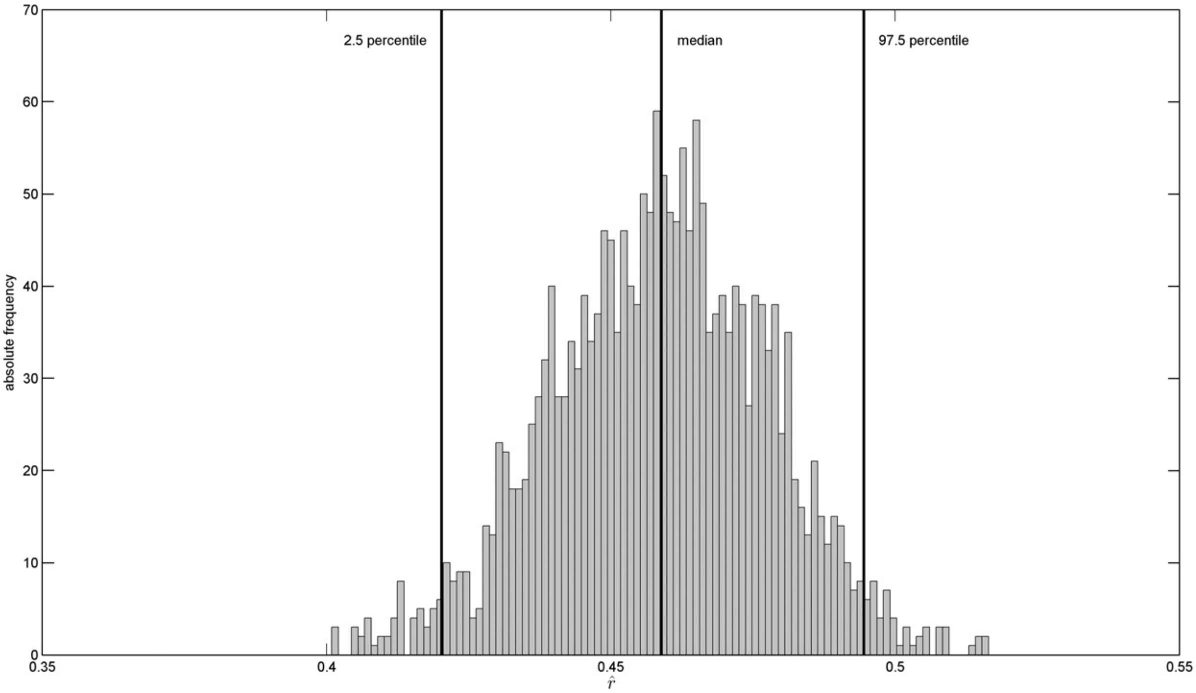

Fig. 3. Histogram of a bootstrap result of the correlation coefficient between TOMS-AI in the Bodélé Depression and SLP at 25°N, 20°E.

coefficient of a bivariate series. The method is aimed at time series with unequal sampling interval but is applicable to equally spaced time series, too. Hereby, both time series are block-wise resampled with replacement until the resampled series has as many observations as the original series. From the resampled series the correlation coefficient is calculated and then the procedure is repeated (bootstrap replications). The block length is proportional to the maximum duration of persistence of the two time series. According to Mudelsee (2002) the persistence τ of a time series is calculated from a linear first-order autoregressive (AR (1)) process where an observation depends on its own immediate past plus a random component. Mathematically this is expressed as:

$$\hat{\tau} = \frac{-1}{\ln\left(\hat{p}^{1/d}\right)}$$

where:

$$\hat{\rho} = \sum_{i=2}^{n} y(i)y(i-1) \Big/ \sum_{i=2}^{n} y(i-1)^2$$

refers to the usual autocorrelation coefficient estimator for a lag of one time unit for the variable y. d is the time span from observation $i-1$ to i and n is the total number of observations. In order to avoid an underestimation of block length during the analysis we corrected a bias of $\hat{\rho}$ of $-(1+3\rho)/(n-1)$ and chose a block length of four times the persistence time as suggested by Mudelsee (2003). Here we only performed persistence analysis of the TOMS-AI series (see results) which revealed a persistence time of 1.4 and, thus, after round up, a block length of 8 days.

We performed as many as 2000 bootstrap replications which have proven to lead to a sufficiently low "bootstrap noise" (Efron and Tibshirani, 1993; Mudelsee, 2003). The generated distribution of correlation coefficients subsequently can be used to construct equitailed confidence intervals between the percentile points. We calculated the 2.5, 50 and 97.5 percentiles from the distribution in order to gain the 95% bootstrap confidence intervals ($\hat{r}_{25\%}$ and $\hat{r}_{97.5\%}$) and median (c.f. Fig. 3). The median $\hat{r}_{\text{med}}$ hereby serves as an estimator of the true correlation coefficient. Correlation coefficients displayed in Figs. 6 and 7 and commented on in the Results section refer to the median of the bootstrap. Results from the significance tests were displayed only where either the lower confidence interval exceeds an arbitrarily chosen value of 0.2 or the upper confidence interval goes below −0.2.

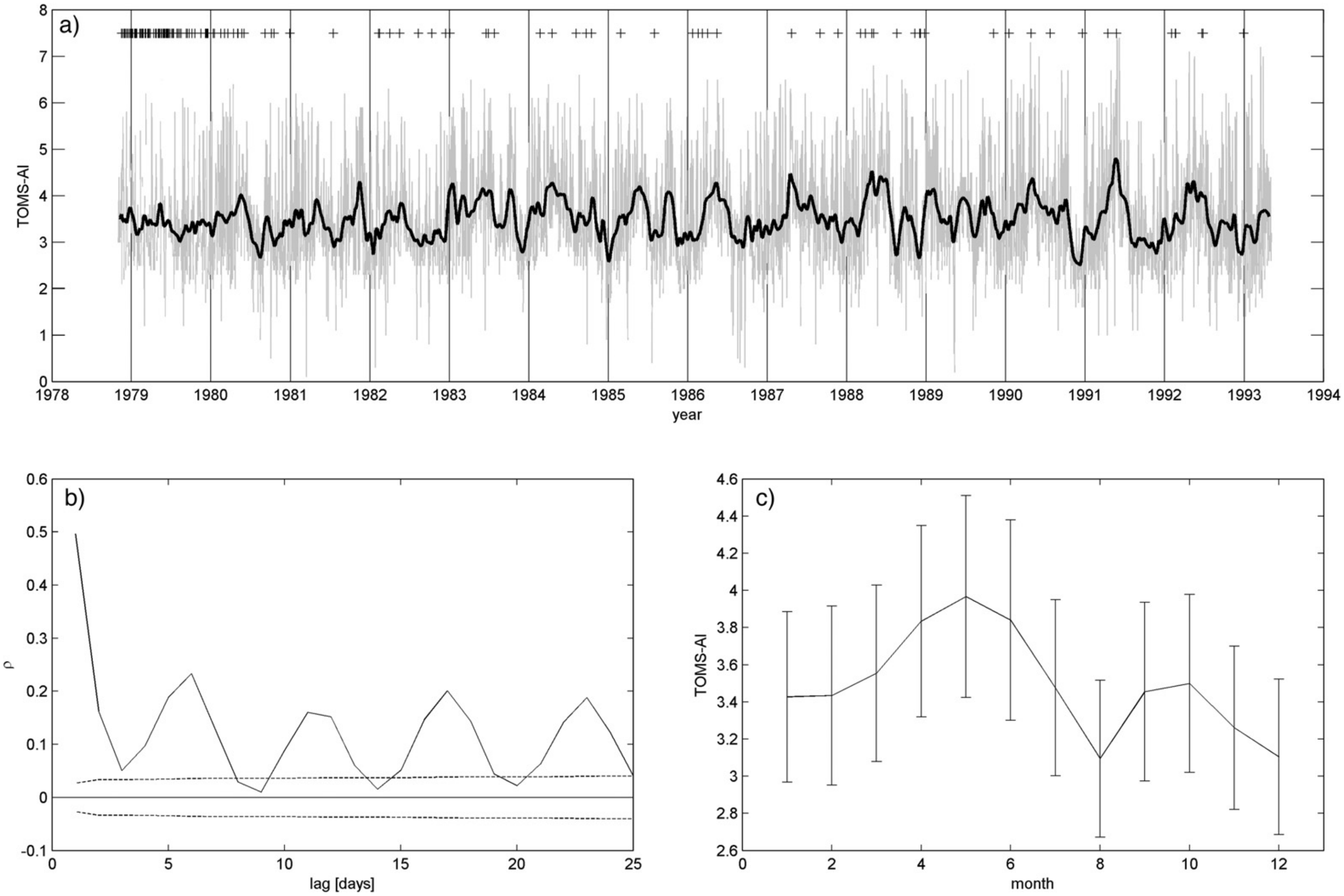

Fig. 4. Analysis of the TOMS-AI time series in the Bodélé Depression in the temporal domain. a) time-variable plot of TOMS-AI. The grey line displays the original time series and the black line shows the low-pass filtered series using a 21-day Gaussian kernel. Black crosses indicate missing values in the time series. b) autocorrelation coefficients of the time series. c) monthly averages of TOMS-AI values and their 95% confidence intervals.

The aforementioned method requires at least weakly stationary time series. An analysis on the temporal behaviour of the TOMS-AI time series in the Bodélé Depression (see results) exhibits a rather complicated seasonal behaviour violating the stationary assumptions. Hence, in order to remove seasonal and trend components from both TOMS-AI series and the meteorological series we applied a temporal forwards and backwards low-pass filter with a 21-day Gaussian kernel to all data prior to the correlation analysis. In a second step the original series was subtracted from the filtered sequence and subsequently z-transformed. This ensures detrended time series with a stationary mean around zero representing the short-term fluctuations of dust emission and atmospheric variability we refer to as large-scale meteorological factors.

The method described above was performed for each grid cell of the NCEP/NCAR reanalysis data for two periods during the year. The first period covers the months December to March and refers to the winter season with high eolian activity when the Harmattan dust is transported south-west from the Bodélé Depression towards the Sahelian and Guinean Coast. The second period investigated is the time from June to August when the TOMS-AI recorded in the Bodélé Depression are low compared to the rest of the year (see Fig. 4c).

4. Results

4.1. Short-term and seasonal variability of TOMS-AI in the Bodélé Depression

Time-variable plots allow several insights into the temporal behaviour of time series. Fig. 4a displays the original and low-pass filtered time series of atmospheric dust in the Bodélé Depression as quantified by TOMS-AI. The time series exhibits no significant trend. The series is marked by strong short-term fluctuations that appear to increase with time. A pattern arising nearly each year is a strong increase in TOMS-AI from December to May as indicated by the low-pass filtered series and the mean monthly values in Fig. 4c. This period is usually followed by a sharp decrease in TOMS-AI during June to August with July being the month with the lowest monthly mean dust concentration

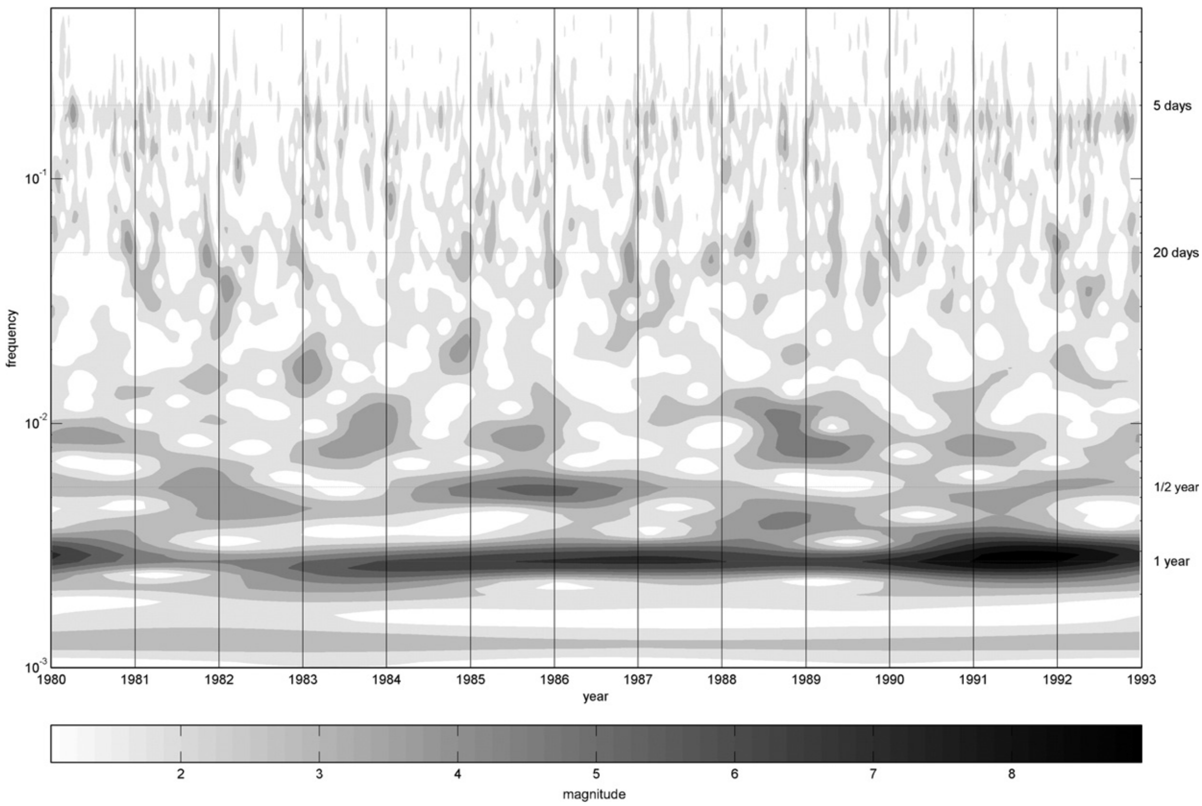

Fig. 5. Morlet wavelet transform (WT) of the TOMS-AI time series in the Bodélé Depression from 1980 to 1992.

as quantified by TOMS-AI. A subsequent increase in TOMS-AI values peaks in October followed by another minimum in December.

The autocorrelation plot in Fig. 4b and a highly significant autocorrelation coefficient of 0.5 for a one-day lag reveals a relatively strong temporal dependence in the TOMS-AI time series in the Bodélé Depression. As the lag number increases a periodic increase and decline of the autocorrelation coefficients with a wavelength of 6 days suggests the presence of a short-term periodicity of the TOMS-AI values in the Bodélé Depression. Though relatively low, autocorrelation coefficients remain significant until a lag number of 60 days.

Both seasonal and short-term periodicities in the TOMS-AI signal as indicated by monthly aggregation and autocorrelation of the TOMS-AI values suggest a superposition of different frequencies in the time series. Their type and occurrence was further investigated using a Morlet WT (Fig. 5) and qualitative interpretation of the wavelet magnitude plot. The abscissa is the timescale, the ordinate corresponds to the frequencies observed and the greyscale responds to the magnitude of the observed frequencies. The WT shows strongest magnitudes for a wavelength around 365 days throughout the whole time of investigation and pronounces the inherent annual cycle in the time series. Highest magnitudes occur during the years 1990 to 1992 where a pronounced seasonal cycle can also be deduced visually from the time series in Fig. 4a. Higher frequencies indicating periodic behaviour of the signal with wavelength around 100 to 200 days are observed during parts of the investigated timespan. An especially strong occurrence of a semi-year cycle is seen during the years 1985 to 1986 where the time series in Fig. 4a exhibits a less pronounced yearly cycle but stronger May and October peaks.

Besides several phases where 20- to 100-day periodicities are recorded, short-term fluctuations greater than a wavelength of five days can be observed throughout the time of investigation. A sharp increase in magnitude is apparent at a wavelength of 6 days that was previously indicated by the autocorrelation analysis (Fig. 4b). The occurrence of these periodicities is most obvious during the first half year of each respective year but appears in several years during late summer and autumn, too. Locally moderate magnitudes at frequencies around 1/10 to 1/20 are discernable.

4.2. Correlation of TOMS-AI and NCEP/NCAR variables

As aforementioned this study focuses on the short-term fluctuations of dust emission in the Bodélé Depression. Hence, the results shown in this subsection are derived from the high-pass filtered series of both variables under investigation as described in the Methods section.

Maps in Fig. 6 show the results of correlation analysis between dust mobilisation and the atmospheric conditions during the winter months (Fig. 6). Isolines of the correlation coefficients estimator $\hat{r}_{\mathrm{med}}$ (hereafter simply termed correlation coefficient) between TOMS-AI and sea level pressure (SLP) sum up to values ranging between 0.3 and 0.5 for the southern Mediterranean coast north of the Bodélé Depression (Fig. 6a). Relatively high SLP is accompanied by two adjoining pressure systems in the 500 hPa-level with increased geopotential heights located above the central Mediterranean Sea and low geopotential heights above the Near East and the Arabian Peninsula (Fig. 6b).

A positive relationship with correlation coefficients exceeding 0.5 exists between TOMS-AI in the Bodélé Depression and wind speed at the 925 hPa level in a zone between the Bodélé Depression and the northern part of the Red Sea (Fig. 6c). A zone with similar extent is characterized by a negative relation between TOMS-AI and air temperature at the 925 hPa level as indicated by correlation coefficients below-0.45. (Fig. 6d). Other meteorological variables investigated but not shown in Fig. 6 exhibit weaker correlation coefficients but partly significantly exceed a modulus of 0.2 (Fig. 8).

During the summer months of June to August correlation coefficients for all variables range between −0.1 and 0.1 and spatial patterns as displayed by the contour lines in Fig. 7 are not apparent.

Results of significance tests on the bootstrapped correlation coefficients calculated for the winter months are displayed in Fig. 8. Each variable shows several cells with significant correlation coefficients with a modulus greater than 0.2. The patterns found in selected variables and pressure levels (Fig. 6) are further confirmed in other pressure levels. For example, the positive correlation stated between wind velocity at the 925 hPa level northeast to the Bodélé Depression and TOMS-AI can also be found at the 850 and 500 hPa level. The same holds true for the inverse temperature-TOMS-AI relationship passing through several pressure levels.

A visual comparison of time series exhibiting highest correlations in winter 1982/83 is shown in Fig. 9. Clearly, the variance of TOMS-AI in the Bodélé is best described by the wind velocity in the 925 hPa located above south-east Egypt. Major peaks in TOMS-AI are well represented in this time series, too. These peaks are less pronounced in the sea level pressure time series

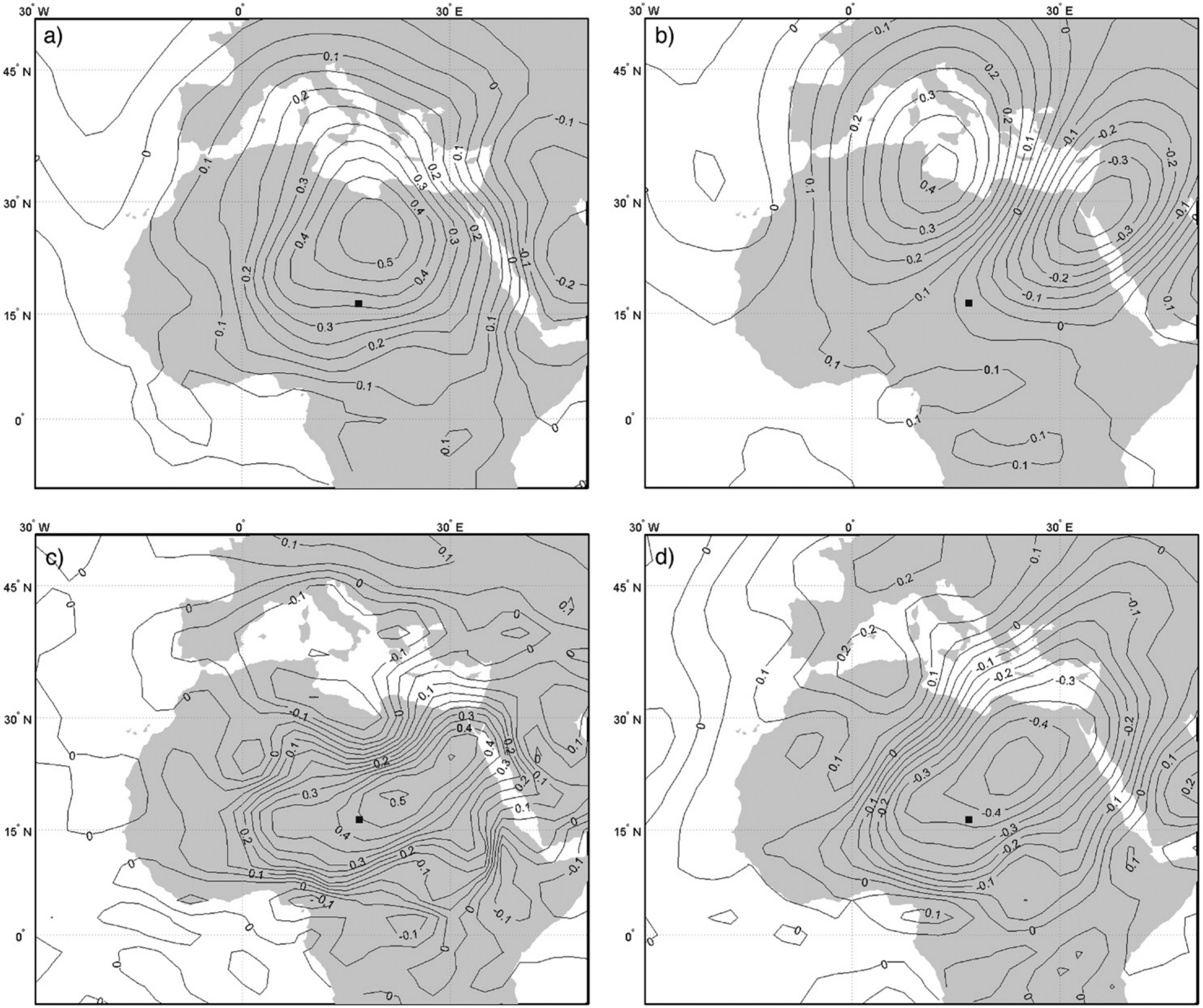

Fig. 6. Estimated correlation coefficients ($\hat{r}_{\mathrm{med}}$) of TOMS-AI in Bodélé and NCEP/NCAR data during December to March for the years 1978–1993. (a) Sea level pressure, (b) 500 hPa geopotential height, (c) 925 hPa wind speed and (d) 925 hPa temperature. The square indicates the location of the Bodélé Depression.

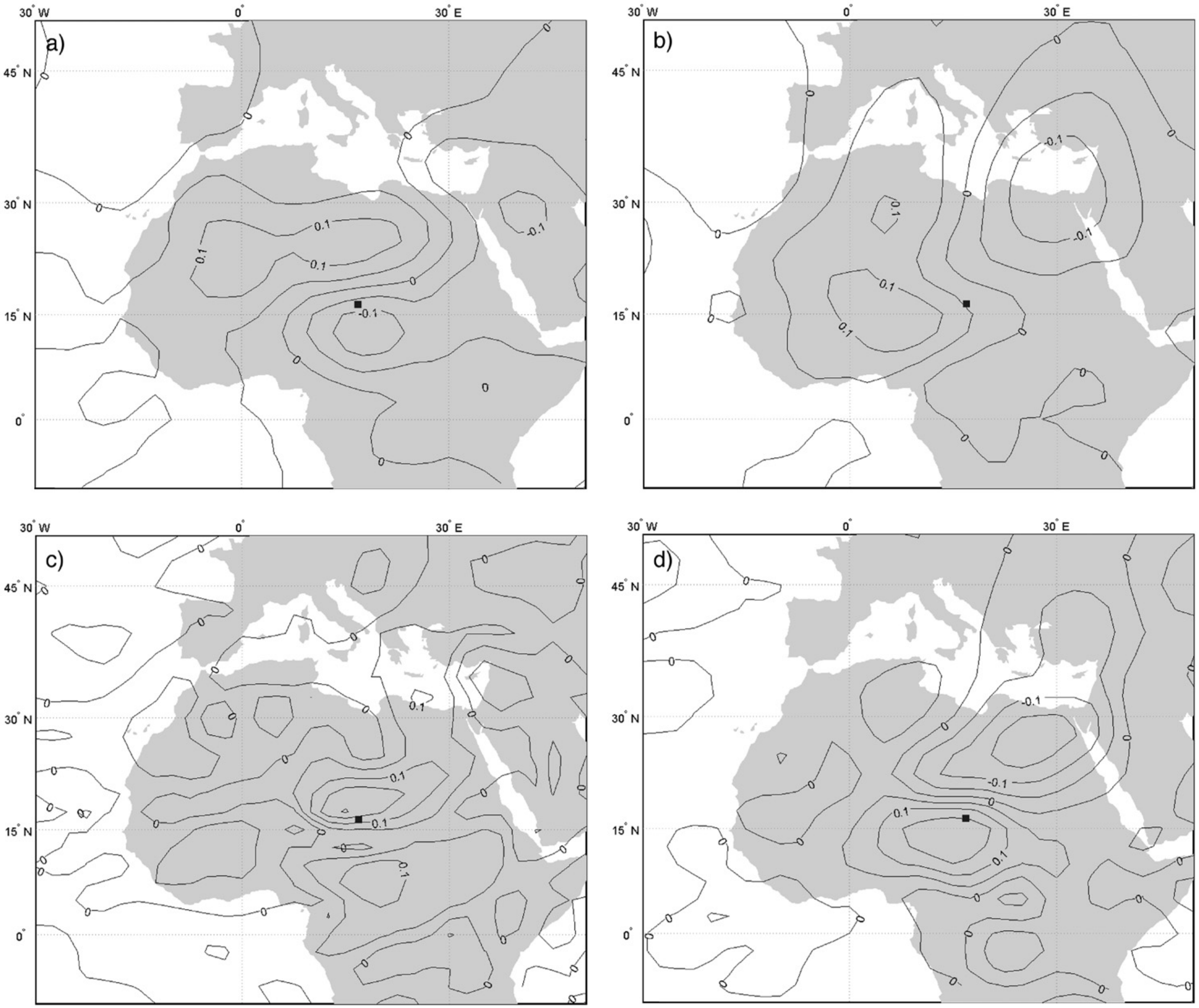

Fig. 7. Estimated correlation coefficients ($\hat{r}_{med}$) of TOMS-AI in Bodélé and NCEP/NCAR data during June to August for the years 1979–1992. (a) Sea level pressure, (b) 500 hPa geopotential height, (c) 925 hPa wind speed and (d) 925 hPa temperature. The square indicates the location of the Bodélé Depression.

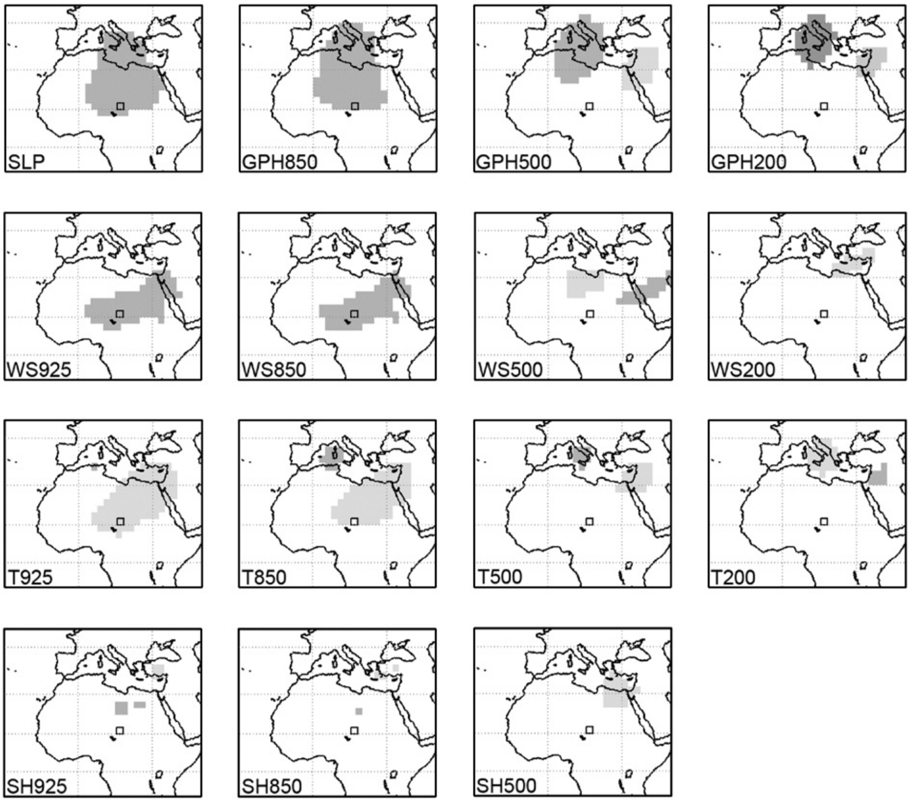

Fig. 8. Significance tests on correlation coefficients for the winter months. Dark grey colors refer to lower confidence intervals greater 0.2 ($\hat{r}_{2.5\%} > 0.2$) and light grey colors refer to upper confidence intervals less than −0.2 ($\hat{r}_{97.5\%} < -0.2$).

above the Libyan coast, which resembles a smoothed representation of the TOMS-AI curve. Positive peaks in the TOMS-AI time series are often accompanied by negative peaks in the temperature curve at the 925 hPa level in the northern Bodélé.

5. Discussion

5.1. Variability of dust emissions from the Bodélé Depression

Several authors have shown that North African atmospheric dust concentrations vary both in time and space (Engelstaedter et al., 2006, and authors therein). We turned our attention to the variability of dust emission of the Bodélé Depression using a wavelet analysis of TOMS-AI data, a method that provides insight both in frequencies of time series and their temporally local occurrence (Lau and Weng, 1995). One daily overpass by the Nimbus satellite as well as a time series length of 15 years, however, leads to constraints regarding the observed frequency ranges of dust mobilisation. The variations in dust emission from the Bodélé Depression investigated here are, therefore, limited from day-to-day variability to seasonal variability. A diurnal cycle of dust mobilization that has been previously recognized by N'Tchayi Mbourou et al. (1997) and Washington et al. (2006) could not be analyzed by the available dataset. For a detection of significant interannual and multiannual fluctuations and trends the Nimbus dataset is to short.

The Morlet WT (Fig. 5) provides evidence for the superposition of various frequencies in dust emission in the Bodélé. The frequency with the greatest magnitude in the time series is the annual cycle driven by the seasonal shift of the pressure belts. The annual cycle is overlain by several intra-annual cycles ranging in wavelengths from 100 days to half a year. These semi-annual cycles constitute in two major periods during the year of increased dust concentrations in the Bodélé Depression as can be deduced from both Fig. 4a and c. First, there is a strong increase from December to May and, second, a weaker increase in September and October that succeeds a decline from June to August. This pattern is not apparent throughout the whole time of investigation. Some years (e.g. 1991) lack such a

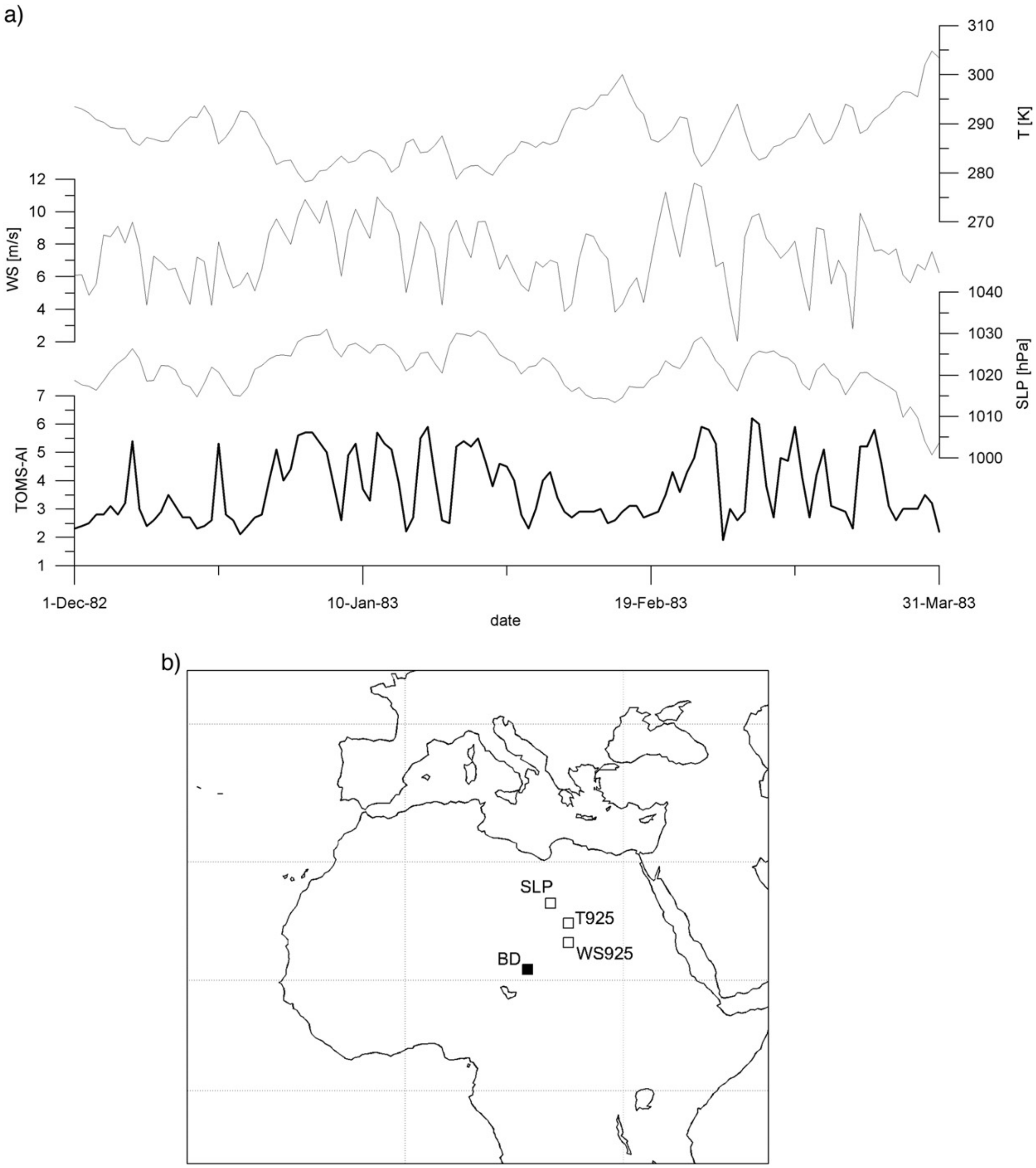

Fig. 9. a: Time series of TOMS-AI in the Bodélé, sea level pressure (SLP, 25°N 20°E), wind speed in 925 hPa (WS925, 20°N 22.5°E) and temperature in 925 hPa (T925, 22.5°N 22.5°E). b: Locations of time series shown in Fig. 5a.

cycle mainly due to an absence of an increased dust emission in autumn following the less dusty conditions during the summer months.

The strong increase in dust emission from December to May has been noted previously by several authors (c.f. Engelstaedter et al., 2006). However, it largely remains unclear, why the TOMS-AI has a maximum located in May in particular regard to observations on dust plumes that suggest a predominant dust emission and strongest wind speeds during the winter months (Washington et al., 2006). As it has been shown by Herman et al. (1997) and Mahowald and Dufresne (2004) TOMS-AI not only depends on dust concentrations but also on aerosol layer height. Hence, we hypothesize that this particular increase in TOMS-AI from January to May is largely due to a heightening of the convection layer caused by the northward shift of the ITCZ during winter and spring months and a subsequent increasing thickness of the atmospheric dust layer above the Bodélé.

Intraseasonal variability of dust concentrations recorded in the Bodélé is recognized by the WT analysis for wavelengths between 6 to 20 days. The ∼20 day wavelengths predominantly occur during the end of the year and are especially apparent during 1980 to 1982 and 1984 to 1988. These frequencies, however, have not been reported in literature before and the reasons for their occurrence remain unclear. Hence, we assume that they relate to wind regime changes in the course of manifestations of the macro-atmospheric conditions during the relatively abrupt displacement of the quasi-permanent circulation systems from summer to winter (Hastenrath, 1988).

Periodicities around 6 days are found in the TOMS-AI time series both in the autocorrelation plot (Fig. 4b) and the WT (Fig. 5). The WT hereby shows a predominant occurrence of this interdiurnal variability during the winter and spring month and partly in autumn. We will focus on this short-term variability of dust mobilisation and its meteorological causes in the next section.

5.2. Correlation of dust entrainment and meteorological settings

The findings from the WT regarding the interdiurnal variability of dust emission in the Bodélé suggest that controls on dust entrainment are substantially different in winter and summer. Although the WT applied here does not provide any means to test the significance of the periodicities found in the TOMS-AI time series, the repeated occurrence of interdiurnal cycles during the winter months and their absence during the summer months is a striking feature characterizing dust emission in the Bodélé.

The seasonal dependence of interdiurnal variability is largely due to the seasonality in the governing wind systems. As aforementioned we performed an extensive correlation analysis to identify the large-scale meteorological controls on dust emission in the Bodélé. While during wintertime significant correlations have been found throughout all the meteorological variables under investigation the climatic controls during the summer months were not identifiable.

During the winter months (December to March) significant spatial patterns of correlation between TOMS-AI and NCEP/NCAR data were found in pressure, wind and temperature fields. The findings suggest that dust emission in the Bodélé Depression is largely controlled by the variability of SLP in the south central Mediterranean. Positive anomalies of SLP in this area relate to positive anomalies in daily dust concentrations in the Bodélé Depression. This relation has been previously demonstrated by Kalu (1979), Washington and Todd (2005) and Washington et al. (2006) who highlight the importance of the Libyan High. The variability of SLP above the Libyan Mediterranean coast is largely related to the frontal regime affecting the Mediterranean area during the winter months. Troughs expand southward as far as the Tibesti Mountains and lead to weakening and disturbance of the prevailing trade winds (Tetzlaff, 1982). Tetzlaff (1982) quantifies the recurrence of these troughs with an average number of 1 to 4 during the winter months that corresponds with the results from the wavelet analysis where periods longer than 6 days were recorded.

A re-formation of the Mediterranean anticyclone results in an amplification of the north-south pressure gradient above the Central Sahara and, hence, leads to a strengthening of the trade winds rooted in the northeast African Mediterranean area as captured by the NCEP/NCAR data (see Figs. 6 and 8). The trade winds are characterised by dry and cold air that has intruded from the north in connection with the troughs (Kalu, 1979), a process well described by the meteorological data analysed. These winds are prevalent in the 925 and 850 hPa levels and have been characterised as LLJ by Washington and Todd (2005) and Washington et al. (2006). The LLJ is further strengthened by funnelling due to the orographic effects of the Tibesti Mountains (Mainguet, 1996) when entering the Bodélé Depression. These winds are able to transport huge sand masses that have a strong corrasive effect on the outcropping diatomites in the former lake basin (Washington et al., 2006). Owing to the diatomite's fine-silty to clayey texture, particles can be held in suspension by stormy winds and are transported southwest by the Harmattan winds affecting large parts of southern West Africa (Breuning-Madsen and Awadzi, 2005; Giles, 2005). This continuous removal of particles results in an estimated 1 cm lowering of the Bodélé's surface per decade (Ergenzinger, 1978).

During July to August a decrease in TOMS-AI mean values (Fig. 4c) indicates a less dusty atmosphere in the Bodélé Depression. However, compared to other summer active sources in West Africa, like the prominent

Mali-Mauritanian source (Prospero et al., 2002), the TOMS-AI values in the Bodélé are still high. During this time the ITCZ has its northernmost position and the averaged monthly wind speeds during this time are very low above the Bodélé as the Harmattan winds do not reach the depression (Fig. 1b).

In summer, the lack of significant correlation of TOMS-AI in the Bodélé (Fig. 7) and the large-scale meteorological factors provides evidence that the daily variability of dust concentrations cannot be explained by the NCEP/NCAR dataset. Thus, it is suggested that dust emission in the Bodélé is uncoupled from the synoptic atmospheric state but reacts to regional or local wind systems during summer. The importance of these micro- to meso-scale systems has been explained by Jäkel and Dronia (1976) and Jäkel (2004) for the Sahara. They show that local to regional surface temperature contrasts induced by different heat conductivities of substrates, variable reflectivity of surfaces and locally varying heating due to shadowing of clouds produce strong enough pressure gradients to generate wind speeds that entrain dust. The extreme reflectivity of the diatomite outcrops in the Bodélé might play an important role for generating regional pressure gradients. Yet, these turbulences obviously remain elusive for a global meteorological dataset like NCEP/NCAR due to their sub-grid size nature but also due to the sparse meteorological observation network in this area. Moreover, severe dust storms in summer are often attributed to downdrafts from convection cells and squall lines (SL) (Hastenrath, 1988; Chen and Fryrear, 2002). Although it has been found that SLs are related to African Easterly Waves, the down-scale interactions from the synoptic-scale waves to the mesoscale SL system remain largely unclear (Fink and Reiner, 2003).

Another factor, however, might significantly influence the results of the correlation analysis. Herrmann et al. (1999, p. 149) notes that "not every dust cloud detected by remote sensing marks a relevant source area". For example, advection of atmospheric dust in higher pressure levels from dust sources in the eastern Sahara (Prospero et al., 2002) might highly influence the TOMS-AI values in the Bodélé Depression and mix with locally entrained dust. The signal caused by this dust is to be considered very strong due to the correlation of TOMS-AI with the aerosol layer height (Herman et al., 1997; Mahowald and Dufresne, 2004). The importance of this background dust (Carlson and Benjamin, 1980) is obvious when one regards the far lower monthly mean frequency of large dust plumes during summer than during winter (Washington and Todd, 2005).

We demonstrate that day-to-day variability in the winter months can be partly explained by sea level pressure (SLP) variability in the Mediterranean area north of the Bodélé Depression in winter. Unexplained variance of TOMS-AI in the Bodélé is thought to be due to several factors. First, the climate observation network in the Sahara is poorly developed. Hence, uncertainty in meteorological predictor variables as described by Koren and Kaufman (2004) needs to be considered. Second, the temporal and spatial resolution of the analysed data does not capture the diurnal cycle of dust emission (N'Tchayi Mbourou et al., 1997; Washington et al., 2006) and its controls, but rather integrates these variables in time and space. Third, it is shown that TOMS-AI not only depends on dust concentrations but also on aerosol layer height (Herman et al., 1997; Mahowald and Dufresne, 2004), a variable that could not be included in the analysis. Furthermore, large uncertainty in dust detection below 1–1.5 km height above ground exists (Chiapello et al., 1999; Prospero et al., 2002) which might introduce large error in the estimation of atmospheric dust concentrations by TOMS-AI.

5.3. Geomorphological significance of findings

The presented linkages between the synoptic weather conditions and dust mobilization depict the variety of temporal and spatial scales involved in the geomorphological processes of particle formation, dust entrainment and dispersion, transport and deposition (Goudie, 1978; Middleton, 1997; Besler, 1992; Pye, 1995). It is shown that the application of large-scale remotely sensed data and global atmospheric datasets enables the documentation and examination of dust-transport processes which up to now have mostly been concluded from geomorphological forms and deposits. Moreover, the findings point to the general predictability of dust spells generated in the Bodélé Depression using global meteorological forecast models. A general improvement in forecast certainty, however, may be achieved when taking the spatial structure of the atmospheric variables into account. Yet, modelling point sources of dust using the 4-dimensional information (including time) in global circulation models remains a challenging task for geomorphologists and meteorologists. Still, the study has also shown that the small-scale view is insufficient to understand the highly complex nature of aeolian dust redistribution but that the integration of local, regional and global-scale observations is required to fully capture the phenomena.

6. Conclusions

We showed that the processes behind dust mobilisation in the Bodélé Depression greatly differ in summer and winter. While the emission of the Harmattan dust is governed by sea level pressure variability in the southern Mediterranean area during the winter months, the controlling meteorological factors in summer are most probably triggered by local and regional wind systems with spatial and temporal extents that cannot be captured by the NCEP/NCAR reanalysis data. Hence, we can partly explain the occurrence of Harmattan dust events, a valuable step forward in the prediction of these severe weather conditions.

The good correlations of the TOMS-AI and NCEP/NCAR variables further show that this global meteorological dataset performs well in capturing the circulation patterns in the remotest areas of the Sahara. However, in order to fully understand the mechanisms behind dust emissions, local and regional effects on wind systems and their controls need to be further investigated.

Acknowledgements

Since February 2005 the German Research Foundation (DFG) has funded the Limnosahara research project (Schu 949-8). Furthermore the first author likes to express his gratitude to Manfred Mudelsee from the Institute of Meteorology, University of Leipzig, and to Jay R. Herman from the NASA Goddard Space Flight Center.

References

Adedokun, J.A., Emofurieta, W.O., Adedeji, O.A., 1989. Physical, mineralogical and chemical properties of Harmattan dust at Ile-Ife, Nigeria. Theoretical and Applied Climatology 40, 161–169.

Arimoto, R., 2001. Eolian dust and climate: relationships to sources, tropospheric chemistry, transport and deposition. Earth-Science Reviews 54, 29–42.

Besler, H., 1992. Geomorphologie der ariden Gebiete. Erträge der Forschung, vol. 280. Darmstadt. [*in german*].

Breuning-Madsen, H., Awadzi, T.W., 2005. Harmattan dust deposition and particle size in Ghana. Catena 63, 23–38.

Brooks, N., Legrand, M., 2000. Dust variability over northern Africa and rainfall in the Sahel. In: McLaren, S., Kniveton, D. (Eds.), Linking Climate Change to Land Surface Change. Kluwer Academic Publishers, Dordrecht, pp. 1–25.

Busche, D., 1998. Die zentrale Sahara. Oberflächenformen im Wandel. Justus Perthes, Gotha. [*in german*].

Carlson, T.N., Benjamin, S.G., 1980. Radiative heating rates for Saharan dust. Journal of the Atmospheric Sciences 37, 193–213.

Chen, W., Fryrear, D.W., 2002. Sedimentary characteristics of a haboob dust storm. Atmospheric Research 61, 75–85.

Chiapello, I., Moulin, C., 2002. TOMS and METEOSAT satellite records of the variability of Saharan dust transport over the Atlantic during the last two decades (1979–1997). Geophysical Research Letters 29 (8), 17.1–17.4.

Chiapello, I., Prospero, J.M., Herman, J.R., Hsu, N.C., 1999. Detection of mineral dust over the North Atlantic Ocean and Africa with the Nimbus 7 TOMS. Journal of Geophysical Research 104 (D8), 9277–9291.

Drake, N., Bristow, C., 2006. Shorelines in the Sahara: geomorphological evidence for an enhanced monsoon from palaeolake Megachad. The Holocene 16, 901–911.

Dunion, J.P., Velden, C.S., 2004. The impact of the Saharan air layer on Atlantic tropical cyclone activity. Bulletin of the American Meteorological Society 85, 353–365.

Efron, B., 1979. Bootstrap methods: another look at the jackknife. Annuals of Statistics 7, 1–26.

Efron, B., Tibshirani, R.J., 1993. An introduction to the bootstrap. Chapman & Hall, London.

Engelstaedter, S., Tegen, I., Washington, R., 2006. North African dust emissions and transport. Earth-Science Reviews 79, 73–100.

Ergenzinger, P.J., 1978. Das Gebiet des Enneri Misky im Tibesti-Gebirge, République du Tchad. Erläuterungen zu einer geomorphologischen Karte 1:200 000. Berliner Geographische Abhandlungen, vol. 23. [*in german with english abstract*].

Fink, A.H., Reiner, A., 2003. Spatiotemporal variability of the relation between African Easterly Waves and West African Squall Lines in 1998 and 1999. Journal of Geophysical Research 108 (D11) ACL5.1-5.17.

Giles, J., 2005. The dustiest place on earth. Nature 434, 816–819.

Gillette, D.A., Chen, W., 1999. Size distributions of saltating grains: an important variable in the production of suspended particles. Earth Surface Processes and Landforms 24, 449–462.

Goudie, A.S., 1978. Dust storms and their geomorphological implications. Journal of Arid Environments 1, 291–310.

Goudie, A.S., Middleton, N.J., 2001. Saharan dust storms: nature and consequences. Earth-Science Reviews 56, 179–204.

Griffin, D.W., Garrison, V.H., Herman, J.R., Shinn, E.A., 2004. African desert dust in the Caribbean atmosphere: Microbiology and public health. Aerobiologica 17, 203–213.

Grove, A.T., Warren, A., 1968. Quaternary landforms and climate on the south side of the Sahara. The Geographical Journal 134, 194–208.

Hastenrath, S., 1988. Climate and circulation of the tropics. D. Reidel Publishing Company, Kluwer, Dordrecht.

Herman, J.R., Bhartia, P.K., Torres, O., Hsu, C., Seftor, C., Celarier, E., 1997. Global distribution of UV-absorbing aerosols from Nimbus 7/TOMS data. Journal of Geophysical Research 102 (D14), 16911–16922.

Herrmann, L., Stahr, K., Jahn, R., 1999. The importance of source region identification and their properties for soil-derived dust: the case of Harmattan dust for easter West Africa. Contributions to Atmospheric Physics 72, 141–150.

Jäkel, D., 2004. Observations on the dynamics and causes of sand and dust storms in arid regions, reported from North Africa and China. Die Erde 135, 341–367 [*in german with english abstract*].

Jäkel, D., Dronia, H., 1976. Ergebnisse von Boden-und Gesteinstemperaturenmessungen in der Sahara. Arbeitsberichte aus der Forschungsstation Bardai/Tibesti. Berliner Geographische Abhandlungen, vol. 24, pp. 55–66. [*in german with english abstract*].

Kalnay, E., Kanamitsu, M., Kistler, R., Collins, W., Deaven, D., Gandin, L., Iredell, M., Saha, S., White, G., Woollen, J., Zhu, Y., Chelliah, M., Ebisuzaki, W., Higgins, W., Janowiak, J., Mo, K.C., Ropelewski, C., Wang, J., Leetmaa, A., Reynolds, R., Jenne, R., Joseph, D., 1996. The NCEP/NCAR 40-Year Reanalysis Project. Bulletin of the American Meteorological Society 77, 437–471.

Kalu, A.E., 1979. The African Dust Plume: its characteristics and propagation across West Africa in winter. In: Morales, C. (Ed.), Saharan Dust. Mobilization, Transport, Deposition. Papers and Recommendations from a Workshop held in Gothenburg, Sweden, 25-28 April 1977, Chichester, New York, Brisbane, Toronto, pp. 95–118.

Koren, I., Kaufman, Y.I., 2004. Direct wind measurements of Saharan dust events from Terra and Aqua satellites. Geophysical Research Letters 31 (L06122), 1–4.

Koren, I., Kaufman, Y.J., Washington, R., Todd, M.C., Rudich, Y., Martin, J.V., Rosenfeld, D., 2006. The Bodélé depression: a single spot in the Sahara that provides most of the mineral dust to the Amazon forest. Environmental Research Letters 1, 1–5.

Lau, K.-M., Weng, H., 1995. Climate signal detection using wavelet transform: how to make a time series sing. Bulletin of the American Meteorological Society 76, 2391–2402.

Mahowald, N.M., Dufresne, J.-L., 2004. Sensitivity of TOMS aerosol index to boundary layer height: Implications for detection of mineral aerosol sources. Geophysical Research Letters 31 (L03103), 1–4.

Mainguet, M., 1996. The Saharo-Sahelian global wind action system: one facet of wind erosion analysed at a synoptic scale. In: Buerkert, B., Allison, B.E., Oppen, M.V. (Eds.), Wind erosion in West Africa: the problem and its control; proceedings of the international symposium, University of Hohenheim, Germany, 5-7 December 1994, Weikersheim, Germany, pp. 7–22.

McPeters, R.D., Bhartia, P.K., Krueger, A.J., Herman, J.R., Wellemeyer, C.G., Seftor, C.J., Jaross, G., Torres, O., Moy, L.G.L., Byerly, W., Taylor, S.L., Swissler, T., Cebula, R.P., 1998. Earth Probe Total Ozone Mapping Spectrometer (TOMS) Data Products User's Guide. Techn. Rep. 1998-206895. National Aeronautics and Space Administration (NASA), Maryland.

McTainsh, G.H., Walker, P.H., 1982. Nature and distribution of Harmattan dust. Z. Geomorph. N.F., vol. 26, pp. 417–435.

Middleton, N.J., 1997. Desert dust. In: Thomas, D.S.G. (Ed.), Arid zone geomorphology. . Process, form and change in drylands, vol. 2. John Wiley & Sons, Chichester, New York, pp. 43–413.

Middleton, N.J., Goudie, A.S., 2001. Sahara dust: sources and trajectories. Transactions of the Institute of British Geographers 26, 165–181.

Morlet, J., 1983. Sampling theory and wave propagation. NATO ASI Series, FI. Springer, pp. 233–261.

Mudelsee, M., 2002. TAUEST: a computer program for estimating persistence in unevenly spaced weather/climate time series. Computers & Geosciences 28, 69–72.

Mudelsee, M., 2003. Estimating Pearson's correlation coefficient with bootstrap confidence interval from serially dependent time series. Mathematical Geology 53, 651–665.

N'Tchayi Mbourou, G., Bertrand, J.J., Nicholson, S.E., 1997. The diurnal and seasonal cycles of wind-borne dust over Africa north of the equator. Journal of Applied Meteorology 36, 868–882.

Pachur, H.-J., Altmann, N., 2006. Die Ostsahara im Spätquartär. Springer, Heidelberg. [*in german*].

Péwé, T.L., 1981. Desert dust: an overview. In: Péwé, T.L. (Ed.), Desert dust: Origin, characteristics, and effect on man. Special Paper of the Geological Society of America, vol. 186, pp. 1–10.

Politis, D.N., 2003. The impact of bootstrap methods on time series analysis. Statistical Science 18, 219–230.

Politis, D.N., Romano, J.P., 1994. The stationary bootstrap. Journal of the American Statistical Association 89, 1303–1313.

Prospero, J.M., 1999. Long-range transport of mineral dust in the global atmosphere: impact of African dust on the environment of southeastern United States. Proceedings of the National Academy of Sciences U.S.A. 96, 3396–3403.

Prospero, J.M., Ginoux, P., Torres, O., Nicholson, S.E., Gill, T.E., 2002. Environmental characterization of global sources of atmospheric soil dust derived from NIMBUS 7 Total Ozone Mapping Spectrometer (TOMS) absorbing aerosol product. Reviews of Geophysics 40 (1), 2.1–2.31.

Pye, K., 1995. The nature, origin and accumulation of Loess. Quaternary Science Reviews 14, 653–667.

Schütz, L., Jaenicke, R., Pietrek, H., 1981. Saharan dust transport over the North Atlantic Ocean. In: Péwé, T.L. (Ed.), desert dust: origin, characteristics, and effect on man. Special Paper of the Geological Society of America 186, 87–100.

Stahr, K., Herrmann, L., Jahn, R., 1996. Long distance dust transport in the Sudano-Sahelian Zone and the Consequences for soil properties. In: Buerkert, B., Allison, B.E., Oppen, M.V. (Eds.), Wind erosion in West Africa: the problem and its control; proceedings of the international symposium, University of Hohenheim, Germany, 5-7 December 1994, Weikersheim, Germany, pp. 23–33.

Tetzlaff, G., 1982. Nordafrikanischer Passat im Winter. Berichte des Instituts für Meteorologie und Klimatologie der Universität Hannover, pp. 22.

Torrence, C., Compo, G.P., 1997. A practical guide to wavelet analysis. Bulletin of the American Meteorological Society 79, 61–78.

Washington, R., Todd, M.C., 2005. Atmospheric controls on mineral dust emission from the Bodélé Depression, Chad: the role of the low level jet. Geophysical Research Letters 32 (L17701), 1–5.

Washington, R., Todd, M., Middleton, N.J., Goudie, A.S., 2003. Dust-storm source areas determined by the total ozone monitoring spectrometer and surface observations. Annals of the Association of American Geographers 93, 297–313.

Washington, R., Todd, M.C., Engelstaedter, S., Mbainayel, S., Mitchell, F., 2006. Dust and the low-level circulation over the Bodélé Depression, Chad: observations from BoDEx 2005. Journal of Geophysical Research 111 (D03201), 1–15.